Cell fragmentation in mouse preimplantation embryos induced by ectopic activation of the polar body extrusion pathway

Diane Pelzer, Ludmilla de Plater, Peta Bradbury, Adrien Eichmuller, Anne Bourdais, Guillaume Halet, Jean-Léon Maître

Article

TRANSPARENT PROCESS OPEN ACCESS

THE EMBO JOURNAL

Cell fragmentation in mouse preimplantation embryos induced by ectopic activation of the polar body extrusion pathway

Diane Pelzer[1], Ludmilla de Plater[1], Peta Bradbury[1], Adrien Eichmuller[1], Anne Bourdais[2], Guillaume Halet[2] & Jean-Léon Maître[1,*]

Abstract

Cell fragmentation is commonly observed in human preimplantation embryos and is associated with poor prognosis during assisted reproductive technology (ART) procedures. However, the mechanisms leading to cell fragmentation remain largely unknown. Here, light sheet microscopy imaging of mouse embryos reveals that inefficient chromosome separation due to spindle defects, caused by dysfunctional molecular motors Myo1c or dynein, leads to fragmentation during mitosis. Extended exposure of the cell cortex to chromosomes locally triggers actomyosin contractility and pinches off cell fragments. This process is reminiscent of meiosis, during which small GTPase-mediated signals from chromosomes coordinate polar body extrusion (PBE) by actomyosin contraction. By interfering with the signals driving PBE, we find that this meiotic signaling pathway remains active during cleavage stages and is both required and sufficient to trigger fragmentation. Together, we find that fragmentation happens in mitosis after ectopic activation of actomyosin contractility by signals emanating from DNA, similar to those observed during meiosis. Our study uncovers the mechanisms underlying fragmentation in preimplantation embryos and, more generally, offers insight into the regulation of mitosis during the maternal-zygotic transition.

Keywords cytoskeleton; meiosis; mitosis; morphogenesis; preimplantation development

Subject Categories Cell Adhesion, Polarity & Cytoskeleton; Cell Cycle; Development

DOI 10.15252/embj.2023114415 | Received 2 May 2023 | Revised 13 June 2023 | Accepted 22 June 2023 | Published online 10 July 2023

The EMBO Journal (2023) 42: e114415

Introduction

Cell fragmentation can lead to the complete disintegration of a cell, aiding clearance during processes such as apoptosis (Atkin-Smith & Poon, 2017). Cell fragmentation can also be partial and contribute to cell and tissue maturation including during germ cell or gonad formation in *Caenorhabditis elegans* embryos (Abdu *et al*, 2016; Lee *et al*, 2019), or the deposition of signaling migrasomes during zebrafish gastrulation (Jiang *et al*, 2019). In other instances, the function and/or benefit of cell fragmentation remains unclear. Interestingly, fragmentation is commonly observed during the preimplantation development of human embryos and is correlated with a poor implantation outcome in assisted reproductive technologies (ART). In human embryos, fragmentation is often associated with chromosome mis-segregation and the formation of micronuclei, negatively affecting further embryonic development (Alikani, 1999, 2007; Fujimoto *et al*, 2011). Importantly, fragmentation in human embryos occurs naturally (Pereda & Croxatto, 1978) and independently of apoptosis (Hardy, 1999). Previous observations in human embryos proposed that membrane threads connected to the zona pellucida (ZP) surrounding the embryo would pull on cells' surfaces and induce fragmentation (Derrick *et al*, 2017). However, fragmentation still occurs when the ZP is removed, suggesting that other mechanisms are at play (Yumoto *et al*, 2020). Aberrant mitoses and malfunctions of the actin and microtubule cytoskeletons were broadly pointed as potential culprits for fragmentation without delineating a clear mechanism (Alikani, 1999; Fujimoto *et al*, 2011; Daughtry *et al*, 2019). While cell fragmentation is frequently observed in human embryos and has been reported in rhesus monkey embryos (Hurst *et al*, 1978; Daughtry *et al*, 2019), it is rarely observed in other mammalian species including mice (Chavez *et al*, 2012) – the typical model used to study human preimplantation development (Wamaitha & Niakan, 2018; Firmin & Maître, 2021). Therefore, identifying mouse mutants that recapitulate human embryo fragmentation would serve as a useful model to dissect the molecular and cellular mechanisms underlying fragmentation during mammalian preimplantation development.

Results

While studying preimplantation morphogenesis, we serendipitously found that loss of unconventional myosin-Ic (Myo1c) causes partial fragmentation in mouse embryos. Myo1c, one of the two Myo1

1 Institut Curie, PSL Research University, CNRS UMR 3215, INSERM U934, Paris, France
2 Institut de Génétique et Développement de Rennes, Université de Rennes, CNRS UMR 6290, Rennes, France
*Corresponding author. Tel: ++33 156246211; E-mail: jean-leon.maitre@curie.fr

paralogs expressed during early preimplantation development (Deng *et al*, 2014; Fig EV1A), tethers actin filaments to phosphatidylinositol 4,5-biphosphate-containing membranes (McIntosh & Ostap, 2016; Lebreton *et al*, 2018), which are found at the plasma membrane of preimplantation embryos (Halet *et al*, 2008). The function of Myo1c has been studied in mammalian cells *in vitro* (Capmany *et al*, 2019; Mangon *et al*, 2021) as well as *in vivo* in flies (Lebreton *et al*, 2018) but its role during mammalian development remains unknown. We find that zygotic KO of Myo1c (Myo1cKO) after CRISPR/Cas9 microinjection causes embryos to form numerous large fragments (Fig 1A). In Myo1cKO embryos, fragments were 5–10 times more numerous than in control embryos and sized twice as large (Figs 1A–C and EV1B). Fragments in Myo1cKO morula rarely contained DNA and were found at the apical surface of the embryo (Fig EV1C and D), similar to that described for both human and rhesus monkey embryos (Hardy, 1999; Van Blerkom *et al*, 2001; Daughtry *et al*, 2019). Fragments that contained DNA were found in the blastocoel of both control and Myo1cKO blastocysts (Fig EV1B–D) and are the likely result of complete cell fragmentation triggered by programmed cell death within the inner cell mass (Plusa *et al*, 2008). Therefore, Myo1cKO mouse embryos form fragments sharing the characteristic location and content of those found in human embryos.

Fragmentation in human embryos tends to occur during mitosis and in clusters (Van Blerkom *et al*, 2001). To investigate precisely when fragmentation takes place in Myo1c mutants, we used light-sheet microscopy of Myo1cKO embryos expressing a plasma membrane marker (mTmG) to visualize fragmentation and mCherry-EB3 to identify mitotic cells by the presence of the mitotic spindle. This revealed that few fragments formed during interphase, and most fragmentation events coincided with the presence of the mitotic spindle (Fig 1D and E, and Movie EV2). In addition, we observed that fragments formed both individually and in clusters (Fig 1D and Movie EV2). Therefore, like human embryos, Myo1cKO mouse embryos form fragments during mitosis and in clusters.

After division, fragmenting blastomeres were to some extent able to divide and develop further (Movie EV1). Initially, Myo1cKO embryos contained a similar number of cells to control embryos (Fig EV1B and E) and early developmental processes such as compaction and apicobasal polarization appeared to occur normally (Fig EV1F–H and Movie EV1). However, Myo1cKO embryos eventually failed to form normal blastocysts. At the blastocyst stage, Myo1cKO embryos exhibited reduced cell number compared with control embryos (Fig EV1B and E) and showed impaired lineage specification and lumen formation (Fig EV1I–M). Therefore, as in human embryos (Hardy, 1999; Van Blerkom *et al*, 2001), cell fragmentation in Myo1cKO mouse embryos is not necessarily linked to cell death but is associated with poor-developmental potential to the blastocyst stage.

In summary of the phenotypic analysis of zygotic Myo1cKO embryos, we found that large apical DNA-free fragments form during mitosis without immediately affecting cell viability but compromising preimplantation development, as reported in human embryos. Thus, using Myo1cKO mouse embryos, which form fragments with the attributes of those typically found in human embryos, we set out to dissect the mechanisms of fragmentation in preimplantation embryos.

While imaging the mitotic spindle in Myo1cKO embryos, we noted several differences with the spindle of control embryos (Fig 2A and Movie EV3). In control embryos, the spindle visualized with mCherry-EB3 appeared and persisted for ~50 min whereas, in Myo1c mutants, the spindle lingered for ~80 min (Fig 2B). To further analyze the relationship between spindle persistence and fragmentation, we measured spindle persistence in fragmenting and non-fragmenting cells of Myo1cKO embryos. Fragmenting cells consistently saw their spindle persisting for ~3 h whereas non-fragmenting cells had their spindles disappearing after ~80 min (Fig 2C). Therefore, fragmentation is associated with a spindle lingering for an abnormally long time. To understand the causes underlying the persistence of the mitotic spindle, we further analyzed its shape and dynamics. We noted that the spindle rotated and bent extensively in Myo1cKO embryos when compared with control ones (Fig 2C–E). This could be the result of poor-mitotic spindle anchoring, as described *in vitro* following Myo1c knockdown (Mangon *et al*, 2021). To test if faulty spindle anchoring would cause fragmentation independently of Myo1c KO, we weakened spindle anchoring using Ciliobrevin D to inhibit dynein, the protein responsible for tethering astral microtubules to the cell cortex (Firestone *et al*, 2012; Kotak *et al*, 2012). Embryos treated with Ciliobrevin D prior to cell division showed enhanced persistence and rotation of the mitotic spindle when compared to DMSO-treated embryos (Fig EV2A–D), confirming that inhibition of dynein impaired spindle anchoring. Strikingly, this treatment phenocopied Myo1c knockout and promoted cell fragmentation (Figs 2F and G, and EV2A–D). Together, we find that Myo1c or dynein dysfunctions are two possible disruptions causing both spindle anchoring defects and cell fragmentation, indicating that spindle anchoring defects are involved in fragmentation.

Early divisions of human preimplantation embryos frequently show defective spindles, causing chromosome misalignments and segregation errors (Kalatova *et al*, 2015; Cavazza *et al*, 2021; Currie *et al*, 2022). Since the spindle in Myo1cKO embryos is defective, we suspected that chromosomes may be incorrectly positioned during mitosis. Labeling chromosomes with SiRDNA or H2B–mCherry revealed that chromosomes in Myo1cKO embryos often come in close proximity with the cell cortex (Fig 3A and Movie EV4). However, after tracking chromosome movements relative to the cell surface, we could not detect any difference in this distance between Myo1cKO and control embryos (Fig EV3A). Although chromosome movements could appear erratic in some Myo1cKO cells, this phenotype could not be captured by comparing the variation in chromosome movements between control and Myo1cKO embryos (Fig EV3B). Instead, as already hinted by the extended persistence of mitotic spindles after Myo1c KO (Fig 2B), particularly in the case of fragmenting cells (Fig 2C), we observed that the nuclear envelope, labeled with lamin associated protein 2b fused to GFP (Lap2b–GFP), tended to take longer to reassemble in Myo1cKO embryos as compared to control ones (Fig EV3C and D, and Movie EV5). This suggests that chromosomes spend extended time in the cytoplasm of Myo1cKO embryos and, as a result, appear to come into contact repeatedly with the cell cortex. Previous studies reported that, during mitosis, chromosomes induce the relaxation of the actomyosin cortex when in close proximity to the pole of dividing cells (Sedzinski *et al*, 2011; Kiyomitsu & Cheeseman, 2013; Rodrigues *et al*, 2015; Ramkumar *et al*, 2021). In stark contrast, we noted that when chromosomes neared the cortex of mitotic cells of Myo1cKO embryos, actin accumulated at the cortex, as seen using the

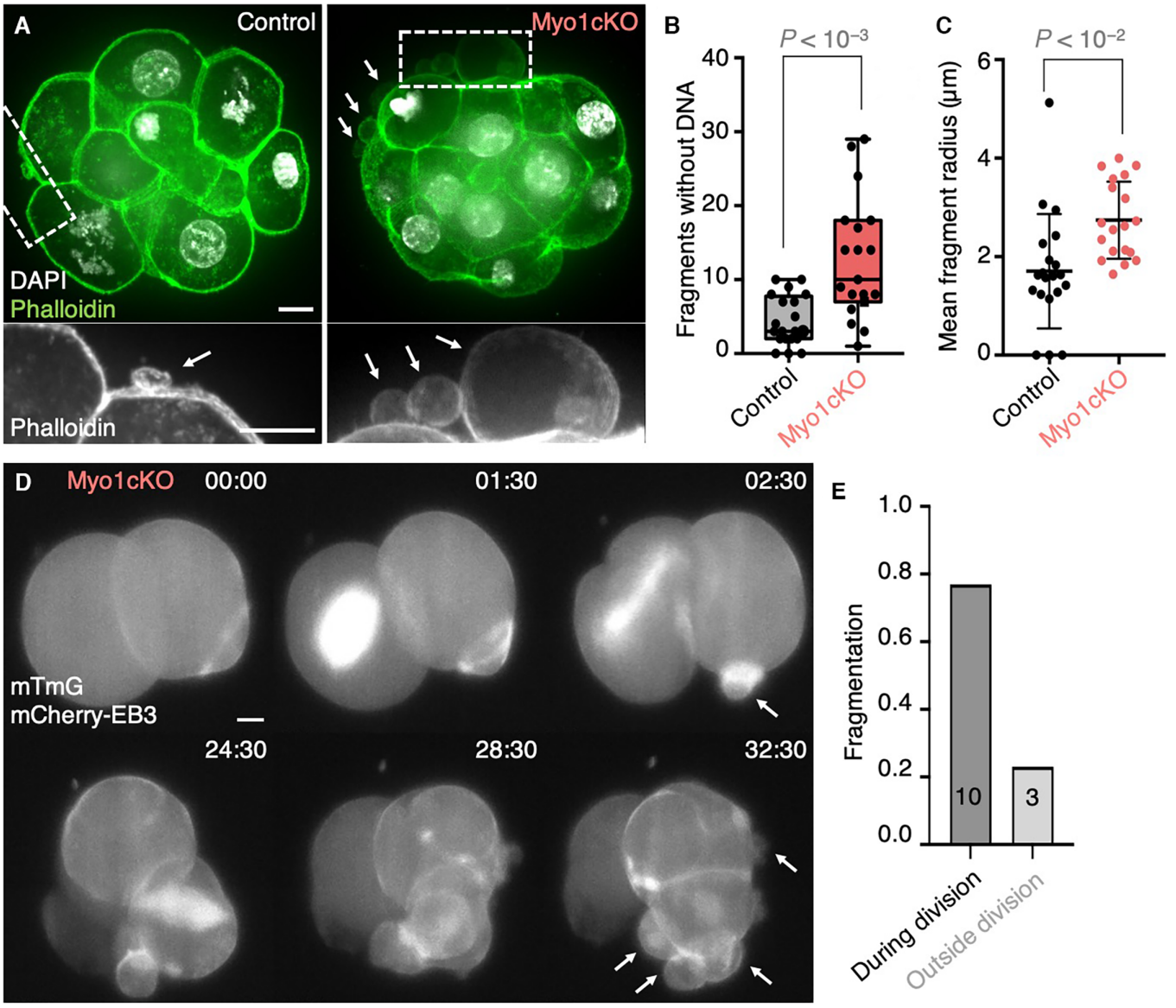

Figure 1. Myo1cKO embryos form fragments.

A Representative image of a Control (left) and Myo1cKO (right) embryo. Top: max projections of embryos stained with Phalloidin (green) and DAPI (gray). Bottom: magnifications at dashed rectangles of Phalloidin (gray) with white arrows pointing at fragments.

B, C Number of fragments without DNA (B) per embryo and mean radius (C) in Control (gray) and Myo1cKO (salmon) embryos (left, Control $n = 20$, Myo1cKO $n = 20$). Boxplot shows median, upper and lower quartiles, min and max values. Whisker plot shows median, upper and lower quartiles.

D Representative images of a time-lapse of a Myo1cKO embryo undergoing fragmentation outside of division (top) and during division (bottom). Max projections of embryos expressing mTmG (gray) and mCherry-EB3 (gray) imaged with light sheet microscopy are shown. White arrows point at the forming fragments.

E Ratio of fragmentation events during and outside of division ($n = 13$ cells from 7 embryos).

Data information: Mann–Whitney test *P*-values are indicated. Scale bars, 10 µm.

filamentous actin reporter LifeAct (Fig 3A–C, and Movies EV4 and EV6). Remarkably, at the poles, non-muscle myosin IIA, the myosin motor-mediating cytokinesis visualized using Myh9–GFP, reached levels comparable to, or higher than that present at the cleavage furrow (Movie EV6). Therefore, not all cells relax their poles during mitosis.

Measuring the local levels of LifeAct–GFP or Myh9–GFP in Myo1cKO embryos revealed increased intensity once DNA came within 20 µm of the cortex (Fig 3B–E). Importantly, the location of Myh9–GFP accumulation corresponded to the site of fragment formation (Fig 3D, and Movies EV4 and EV6). Careful observation of the formation of fragments suggested that Myh9–GFP formed a ring-like structure that 'pinched off' a piece of the cell (Movie EV7). Importantly, when DNA came within close proximity to the cortex, Myh9–GFP accumulation could be detected in both control and Myo1cKO embryos (Fig 3E). However, Myh9–GFP accumulation in

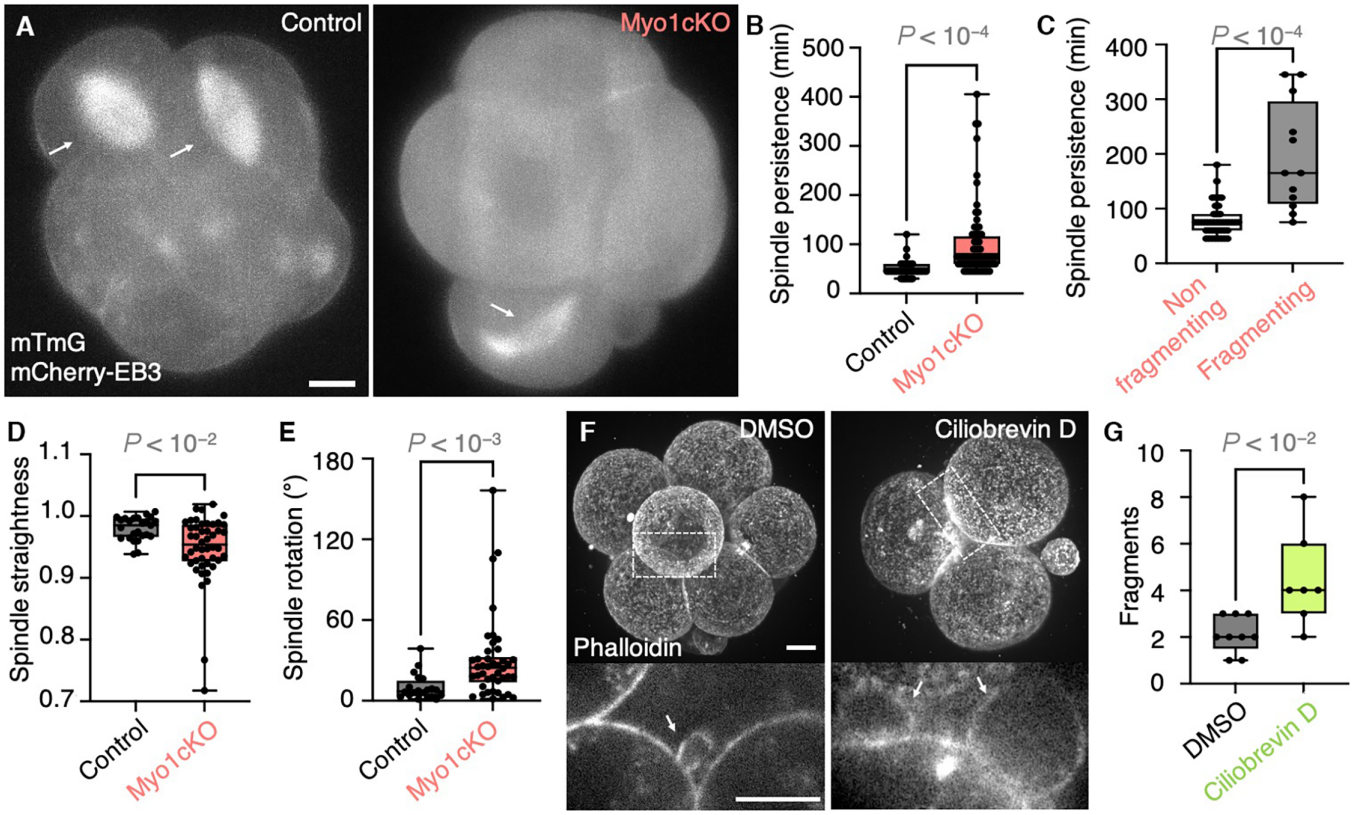

Figure 2. Defective spindle anchoring leads to fragmentation.

A Representative images of Control (left) and Myo1cKO (right) embryos expressing mTmG and mCherry–EB3 (gray) shown as max projections. White arrows indicate the mitotic spindle.

B, C Spindle persistence in Control (n = 6) and Myo1cKO (n = 9) embryos (B) and in non-fragmenting and fragmenting cells of Myo1cKO embryos (C, n = 42 and 12 cells from 7 Myo1cKO embryos). Spindle persistence measures the time from appearance to disassembly of the spindle.

D, E Spindle straightness (D) and rotation (E) in Control (n = 6) and Myo1cKO (n = 9) embryos. Straightness reports the pole to pole distance of the spindle divided by its continuous length. Rotation describes the angle between the initial orientation of the spindle pole and its maximal deviation in 2D.

F Representative images of embryos treated with DMSO (left) and 37.5 μM Ciliobrevin D (right), stained with Phalloidin. Top: Maximum projection. Bottom: magnifications of a single plane at dashed rectangles of Phalloidin with white arrows pointing at fragments.

G Number of fragments without DNA per embryo in DMSO (gray) and Ciliobrevin D (honeydew) embryos at E2.5 (left, Control n = 9, Myo1cKO n = 7).

Data information: the Mann–Whitney test P-values are indicated. Boxplots show median, upper and lower quartiles, min and max values. Scale bars, 10 μm.

control embryos was less pronounced than in Myo1cKO ones (Fig 3F), suggesting that the signaling cascade that induces cortical Myh9 accumulation is more stimulated and/or more responsive in Myo1cKO embryos than in the control. Together, our findings indicate that defective spindles bring chromosomes close to the cortex for an extended duration (Figs 2 and EV2) and coincides with ectopic activation of contractility, causing a small portion of the cell to pinch off, thereby generating a fragment (Fig 3).

The aforementioned series of events described in mitotic cells, strikingly resembles the extrusion of the polar body during meiosis (Uraji *et al*, 2018). In mouse oocytes, the meiotic spindle must migrate toward the cell periphery forcing chromosomes within close proximity of the actomyosin cortex. The meiotic spindles and chromosomes eventually trigger a signaling cascade that assembles an actin cap surrounded by a non-muscle myosin-II ring to pinch off the polar body. Strikingly, the assembly of the actomyosin cap extruding the polar body is induced when chromatin comes within 20 μm of the cortex (Deng *et al*, 2007), a distance similar to that observed prior to fragment formation during cleavage stages (Fig 3B, C and E). Two distinct signals coordinate polar body extrusion (PBE). The first originates from the chromosomes and involves, among other effectors, the small GTPase, Cdc42 to promote actin polymerization (Deng *et al*, 2007; Dumont *et al*, 2007; preprint: Bourdais *et al*, 2022). The second emanates from the central spindle complex, which organizes the contractile cytokinetic ring, via, among other effectors, the Rho Guanine Exchange Factor (GEF), Ect2 (Dehapiot *et al*, 2021). Importantly, the PBE signaling cascade is responsible for both encapsulating half of the maternal genome into the polar body, and also for repelling the remaining maternal chromosomes away from the cortex (Wang *et al*, 2020; Dehapiot *et al*, 2021). In fact, following the completion of meiosis, paternal chromosomes that near the cortex also induce actin caps and can form transient buds in zygotes (Simerly *et al*, 1998; Mori *et al*, 2021). Therefore, the signaling pathway driving PBE remains active hours after the completion of meiosis and it is unclear when this meiotic pathway is terminated.

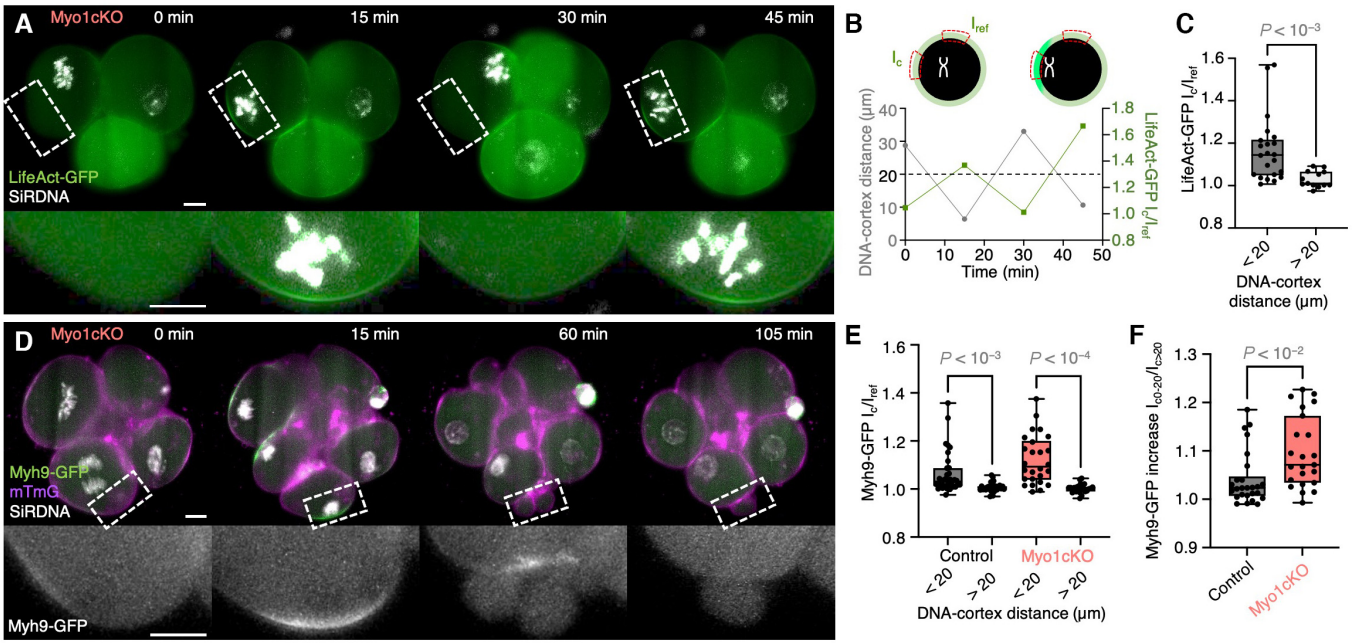

Figure 3. Actomyosin cap formation in proximity of DNA.

A Top: Representative images of a time-lapse of a Myo1cKO embryo labeled with LifeAct–GFP (green) and SiRDNA (gray) with one blastomere undergoing mitosis shown as max projections. Bottom: magnifications of dashed rectangles.

B In Myo1cKO embryo shown in (A) LifeAct–GFP intensities at the cortex region of eventual contact with DNA (I_c) are normalized to the intensity at a reference region (I_{ref}). LifeAct–GFP I_c/I_{ref} values (green) are plotted over time. The DNA-cortex distance (gray) between the region of eventual contact and the center of the DNA signal is also measured. A threshold distance of 20 µm is indicated with a dashed line.

C LifeAct-GFP I_c/I_{ref} values at DNA-cortex distances < 20 and > 20 µm (Myo1cKO embryos n = 13, cells n = 21).

D Top: Representative images of a time-lapse of a Myo1cKO embryo expressing Myh9–GFP (green) and mTmG (magenta) while labeled with SiRDNA (gray) undergoing fragmentation during mitosis shown as max projections. Bottom: magnifications of Myh9-GFP (gray) at dashed rectangles showing cortical accumulation (middle) followed by fragmentation (right).

E Control (gray) and Myo1cKO (salmon) embryos Myh9–GFP I_c/I_{ref} values at DNA-cortex distances < 20 and > 20 µm (Control embryos n = 10, cells n = 35; Myo1cKO embryos n = 9, cells n = 26).

F Comparison of the increase in Myh9–GFP intensity in Control and Myo1cKO embryos when DNA is in close proximity to the cortex. The ratio $I_{c0\text{-}20}/I_{c\ >\ 20}$ is calculated from Myh9–GFP intensities at the contact region when DNA-cortex distances are < 20 µm ($I_{c0\text{-}20}$) divided by intensities when distances are > 20 µm ($I_{c\ >\ 20}$; Control embryos n = 10, cells n = 33; Myo1cKO embryos n = 9, cells n = 26).

Data information: Mann–Whitney test (C, F) or Kruskal–Wallis and pairwise the Mann–Whitney tests (E) P-values are indicated. Boxplots show median, upper and lower quartiles, min and max values. Scale bars, 10 µm.

To test if the PBE pathway is active in cleavage stage embryos and involved in cell fragmentation, we investigated the two signals involved in PBE – those that originate from the chromosomes (via Cdc42) and from the spindle (via Ect2). We monitored Cdc42 activity using a probe that exploits the Cdc42-GTP-binding region of myotonic dystrophy kinase-related Cdc42-binding kinase (MRCK; preprint: Bourdais *et al*, 2022). We observed that the active Cdc42 probe accumulated at the cortex specifically when chromosomes

◀ **Figure 4. The polar body extrusion (PBE) pathway is necessary and sufficient to induce fragmentation during cleavage stages.**

A Representative images of Control (left) and Myo1cKO (right) embryos labeled with SiRDNA (gray) and expressing a reporter of Cdc42 activity (yellow) in one blastomere, which is undergoing mitosis, shown as max projections. The second blastomere is outlined with a dashed line. White arrows point at the accumulation of active Cdc42 at the cortex in close proximity to DNA.

B The ratio of active Cdc42 I_c/I_{ref} was compared between < 20 and 20 µm DNA-cortex distances for Control (dark yellow) and Myo1cKO (yellow) embryos (Control embryos n = 10; Myo1cKO embryos n = 10).

C Representative images of Myo1cKO embryos expressing LifeAct–GFP (green) alone (left) or together with dominant negative Cdc42 (DNCdc42, right) labeled with SiRDNA (gray) shown as max projections. White arrows point at the cortex in close proximity to DNA.

D LifeAct–GFP I_c/I_{ref} values at DNA-cortex distances < 20 and > 20 µm for Myo1cKO (salmon) and Myo1cKO + DNCdc42 (yellow) embryos (Myo1cKO embryos n = 8, cells n = 19; Myo1cKO + DNCdc42 embryos n = 12, cells n = 30).

E Representative images of a GFP (left) and Ect2–GFP (right) expressing embryo stained with Phalloidin (green) and DAPI (gray) shown as max projections. White arrows indicate fragments.

F Number of fragments without DNA per embryo in GFP (gray) and Ect2–GFP (blue) embryos (GFP n = 14; Ect2–GFP n = 18).

Data information: The Kruskal–Wallis and pairwise Mann–Whitney tests (B, D) or Mann–Whitney test (F) P-values are indicated. Boxplots show median, upper and lower quartiles, min and max values. Scale bars, 10 µm.

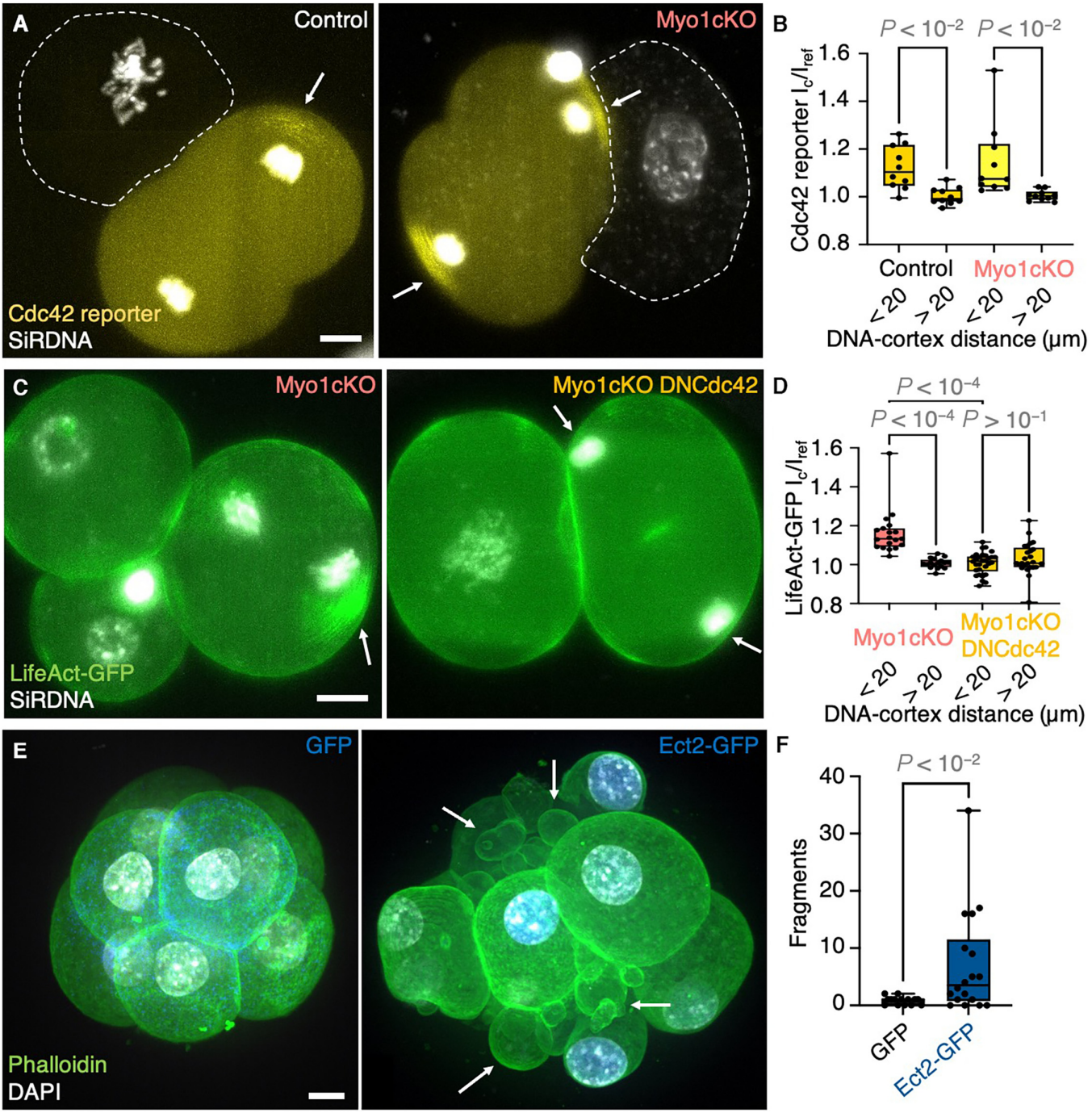

Figure 4.

were within 20 µm (Fig 4A and B, and Movie EV8), suggesting that, like during meiosis, the PBE pathway is active during mitosis. Importantly, Cdc42 was activated in both control and Myo1cKO embryos without necessarily triggering fragment formation, similar to when paternal DNA induces the formation of actin caps without being extruded (Simerly *et al*, 1998; Mori *et al*, 2021). To next determine whether Cdc42 activation is responsible for the chromosome-induced actin accumulation in Myo1cKO embryos, we used a dominant negative Cdc42 (DNCdc42). As described previously, when chromosomes came within 20 µm of the cortex of Myo1cKO embryos, an accumulation of actin was observed (Fig 3A–C) however, this was abolished by the expression of DNCdc42 (Fig 4C and D, and Movie EV9). Therefore, fragmentation of preimplantation embryos is driven by Cdc42-mediated actin polymerization following DNA nearing the cortex. In addition, we investigated signals originating from the mitotic spindle by increasing the levels of Ect2. Expression of Ect2–GFP induced the formation of numerous large fragments, while expression of GFP alone did not (Fig 4E and F).

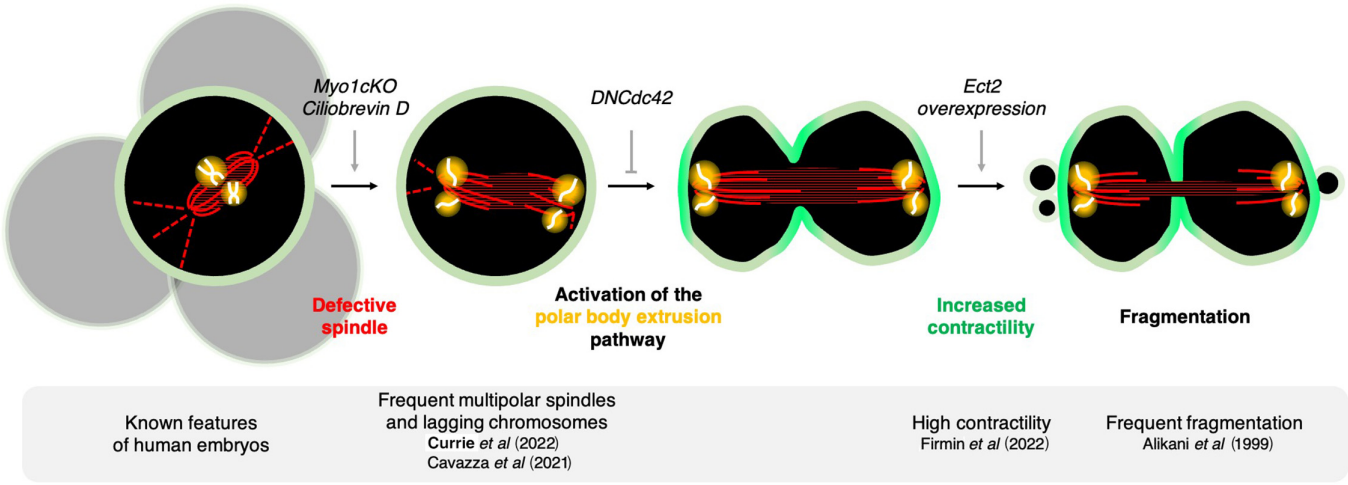

Figure 5. Schematic diagram of the steps leading to cell fragmentation in preimplantation embryos.
Spindle in red, DNA in white, signals from the DNA in yellow and actomyosin in green.

Therefore, increased signaling from Ect2 is sufficient to induce fragment formation. Taken together, we find that core elements of the PBE pathway are active, necessary, and sufficient to induce fragmentation in preimplantation embryos.

Our experiments show that ectopic signals originating from the chromosomes or from the spindle can lead to fragmentation. To dissect the specific mechanisms of action of both signals, we measured actomyosin levels upon DNA nearing the cortex as a readout of PBE pathway activation. In Myo1cKO embryos, Myh9–GFP recruitment was increased compared to control embryos (Fig 3F), which could be explained by the longer persistence of the mitotic spindle dragging the chromosomes throughout the cell (Figs 2B and EV3, and Movies EV3–EV5). Therefore, when the mitotic spindle is poorly anchored, the PBE pathway appears to be hyper-activated compared with control embryos. In Ect2–GFP expressing embryos, actin levels increased when DNA neared the cortex as observed in control embryos (Fig EV4A and B, and Movie EV10). However, in contrast to Myo1c knockout, Ect2–GFP expression did not enhance actin recruitment compared with control embryos (Fig EV4B). Therefore, hyper-activation of the PBE pathway may not be the cause of fragmentation in Ect2–GFP expressing embryos.

Since Ect2 activates Rho, a master regulator of actomyosin contractility (Matthews *et al*, 2012), expression of Ect2–GFP could raise the basal contractility and lower the threshold for fragmentation upon normal activation of the PBE pathway. To assess contractility, we used micropipette aspiration to measure the surface tension of embryos expressing Ect2–GFP (Maître *et al*, 2015). Surface tension of blastomeres expressing Ect2–GFP was increased when compared to GFP-expressing cells (Fig EV4C). In contrast, Myo1cKO embryos displayed surface tensions that were identical to control embryos (Fig EV1G and H). Together, these measurements indicate that fragmentation can occur when contractility is abnormally high, even when the PBE pathway is activated to normal levels. In summary, we observe fragmentation either after hyper-activation of the PBE pathway in cells with normal contractility or after ectopic activation of the PBE pathway in cells with hyper contractility.

Discussion

Taken together, our experiments delineate a mechanism to explain cell fragmentation (Fig 5), a process that is detrimental to human embryonic development and human fertility. We find that fragments form by ectopic contraction of the actomyosin cortex (Fig 3) upon activation of a meiotic pathway that is unexpectedly still operative during mitosis (Fig 4). Specifically, we find that the PBE pathway is engaged, as during meiosis, when chromosomes come near the cortex (Figs 3 and 4). During mitosis, ectopic activation of the PBE pathway is more pronounced when the spindle suffers from poor anchoring (Fig 2). Since human embryos show frequent issues with spindle and chromosome capture (Kalatova *et al*, 2015; Cavazza *et al*, 2021; Currie *et al*, 2022), we propose that fragmentation may result from hyper-activation of the PBE pathway due to problems during chromosome separation. Importantly, ectopic activation of the PBE pathway occurs in control embryos without causing much fragmentation (Figs 3 and 4). However, in embryos with increased basal contractility and surface tension, the same ectopic activation of the PBE pathway triggers fragmentation (Figs 4 and EV4). Interestingly, in a recent study, we measured the surface tension of human embryos and reported tensions 5–10 times higher than for mouse embryos, indicative of high basal contractility in human embryos (preprint: Firmin *et al*, 2022). Thus, with unstable spindles and high contractility, human embryos cumulate two features that could synergistically promote fragmentation (Fig 5). Future studies focusing on reducing contractility and/or PBE pathway activation in human embryos may therefore be key to reduce fragmentation and improve human fertility.

Finally, we uncover novel features of mitotic regulation. We find that not all mitotic cells relax the acto-myosin cortex when chromosomes come near the cortex, contrary to what has been described so far in somatic cells (Sedzinski *et al*, 2011; Kiyomitsu & Cheeseman, 2013; Rodrigues *et al*, 2015; Ramkumar *et al*, 2021). Specifically, we show in cleavage stage embryos, when DNA comes within 20 μm of the cortex, it locally activates Cdc42 and triggers actomyosin contraction (Figs 3 and 4). We propose that this is due to the

persistent activity of the PBE pathway 3 days after completion of meiosis (Fig 4), revealing an unexpected prolongation of maternal processes in the embryo. There may be in fact little pressure to terminate the PBE pathway upon completion of meiosis. Indeed, cleavage stage blastomeres are rather large cells, thereby reducing the risk that a well anchored and centered mitotic spindle would bring chromosomes near the cortex long enough to trigger the PBE pathway. We recently found that, as a result of remodeling of the actomyosin cortex, surface tension decreases concomitantly with cells decreasing in size during cleavage stage embryos (Özgüç *et al*, 2022). This progressive mechanical maternal–zygotic transition may reduce the consequences of the ectopic activation of the PBE pathway and prevent cell fragmentation in mouse embryos. Whether cortical softening occurs in human embryos remains unknown and our findings highlight that much remains to be understood about how embryos transition both molecularly and mechanically from meiotic to mitotic divisions.

Materials and Methods

Embryo work

Recovery and culture

All animal work is performed in the animal facility at the Institut Curie, with permission by the institutional veterinarian overseeing the operation (APAFIS #11054-2017082914226001). The animal facilities are operated according to international animal welfare rules.

Embryos are isolated from superovulated female mice mated with male mice. Superovulation of female mice is induced by intraperitoneal injection of 5 international units (IUs) pregnant mare's serum gonadotropin (PMSG, Ceva, Syncro-part), followed by intraperitoneal injection of 5 IU human chorionic gonadotropin (hCG, MSD Animal Health, Chorulon) 44–48 h later.

Embryos are recovered at E0.5 in 37°C FHM (LifeGlobal, ZEHP-050 or Millipore, MR-122-D) by dissecting, from the oviduct, the ampula, from which embryos are cleared with a brief (5–10 s) exposure to 37°C hyaluronidase (Sigma, H4272).

Embryos are recovered at E1.5 by flushing oviducts from plugged females with 37°C FHM using a modified syringe (Acufirm, 1400 LL 23).

Embryos are handled using an aspirator tube (Sigma, A5177-5EA) equipped with a glass pipette pulled from glass micropipettes (Blaubrand intraMark or Warner Instruments).

Embryos are placed in KSOM (LifeGlobal, ZEKS-050 or Millipore, MR-107-D) or FHM supplemented with 0.1% BSA (Sigma, A3311) in 10 µl droplets covered in mineral oil (Sigma, M8410 or Acros Organics) unless stated otherwise. Embryos are cultured in an incubator with a humidified atmosphere supplemented with 5% CO_2 at 37°C.

To remove the ZP for tension measurements, embryos are incubated for 45–60 s in pronase (Sigma, P8811).

For imaging, embryos are placed in Viventis Microscopy LS1 Live light-sheet chambers or 5 glass-bottom dishes (MatTek).

Only embryos surviving the experiments were analyzed. Survival is assessed by continuation of cell division as normal when embryos are placed in optimal culture conditions.

Mouse lines

Mice are used from 5 weeks old on (C57BL/6xC3H) F1 hybrid strain is used for wild-type (WT). To visualize plasma membranes, mTmG (Gt(ROSA)26Sor$^{tm4(ACTB-tdTomato,-EGFP)Luo}$) is used (Muzumdar *et al*, 2007). To visualize filamentous actin, LifeAct–GFP (Tg(CAG–EGFP)#Rows) is used (Riedl *et al*, 2010). To visualize chromatin, R26-H2B-mCherry CDB0239K is used (Abe *et al*, 2011). To generate embryos with a maternal Myh9–GFP allele, Myh9$^{tm8.1RSad}$ females were mated with WT males (Zhang *et al*, 2012).

Chemical reagents and treatments

Ciliobrevin D (Merck, 250401) 5 mM dimethyl sulfoxide (DMSO) stock was diluted to 37.5 µM in KSOM. Late 2-cell-stage embryos were cultured in 37.5 µM Ciliobrevin D for 1 day. Only those embryos that continued to divide were considered.

For live DNA staining, embryos were incubated in KSOM-containing SiRDNA (Table 1) for 30 min prior to imaging.

Plasmids and mRNA preparation

The following plasmids were used: mCherry-EB3-7 (Addgene 55,037), Ect2-GFP (Dehapiot *et al*, 2021), DNCdc42 (encoding Cdc42 with T17N swap; Dehapiot *et al*, 2013), Cdc42 reporter (preprint: Bourdais *et al*, 2022), LifeAct-GFP, LifeAct-RFP (Riedl *et al*, 2008), and Lap2b-GFP (gift from Maria Almonacid and Marie-Hélène Verlhac). For mRNA generation of mCherry-EB3 and Ect2-GFP, the template was generated by amplification of the fragments encoding mCherry-EB3 or Ect2-GFP, respectively, followed by SV40 PolyA with a forward (fwd) primer containing a T7 site at the 5′ end. The GFP template was generated by amplification of the GFP sequence

Table 1. Information related to fluorescent labeling of fixed and live embryos: name, dilution, provider, and research resource identifier (RRID).

Primary antibodies	Dilution	Provider	RRID
Cdx2	1:200	Abcam ab157524	AB_2721036
Sox2	1:100	Abcam ab97959	AB_2341193
Pard6b	1:50	SantaCruz 166405	
Aqp3	1:500	Novusbio NBP2-33872	

Secondary antibodies and dyes	Dilution	Provider	RRID
Alexa Fluor Plus 488 anti-mouse	1:200	Invitrogen, A32723	AB_2633275
Alexa Fluor 546 anti-mouse	1:200	Invitrogen, A11003	AB_2534071
Alexa Fluor Plus 488 anti-rabbit	1:200	Invitrogen, A32731	AB_2633280
Alexa Fluor Plus 546 anti-rabbit	1:200	Invitrogen, A11010	AB_2534077
Alexa Fluor 633 phalloidin	1:200	Invitrogen, A22284	
4′,6-diamidino-2-phenylindole (DAPI)	1:1,000	Invitrogen, D1306	AB_2629482
SiRDNA	1:1,000	Spirochrome	

from the pCS2-GFP-Fmnl3 with a fwd primer containing the SP6 site. The remaining plasmids were linearized by restriction enzyme digestion. The linear fragments were used as template for mRNA transcription using the mMessage mMachine T7, T3, or SP6 kit (Invitrogen, AM1340, AM1344, AM1348) according to manufacturer's instructions followed by resuspension in RNase free-water.

gRNA design and generation

To target Myo1c a set of two gRNAs for each gene targeting close to the start codon are designed using the web tool CHOPCHOP (Labun *et al*, 2019), namely TGACGGGGTTCGAGTGACCATGG and TTG ACTGCCCGAGACCGGGTAGG. For RNA transcription, the gRNA target sequences are cloned into pX458 (Addgene, 48138) as previously described (Cong *et al*, 2013). Briefly, following digestion of the plasmid with BbsI, two annealed oligos encoding the gRNA target region, containing the 5′ overhang AAAC and the 3′ overhang CAAAAT are phosphorylated and cloned into pX458. The gRNA and its backbone are amplified by PCR with a fwd primer containing a T7 site. Following PCR purification RNA is transcribed using the MEGAshortscript T7 transcription kit (Invitrogen, AM1354). The RNA is then purified by using the MEGAclear kit (Invitrogen, AM1908).

Genotyping

Following imaging, individual embryos are collected for genomic DNA extraction. Single embryos are placed into a genomic DNA extraction buffer (10 mM Tris–pH 8.5, 50 mM KCl, 0.01% gelatin, Proteinase K). Subsequently, a nested PCR was performed to amplify the region surrounding the predicted mutation site using the following primer pairs for Myo1c: fwd: CCTGTAACACGTAGCTGGG A rev: GGGGTTTGGATGGGGTCAT for the first PCR and fwd: GCCTGTGTCCAAAGTGTCCC rev: CCGTGCTCATGGCACTCAC for the second PCR.

WT and mutants were determined by gel electrophoresis. Both homozygous and heterozygous embryos are considered as Myo1cKO embryos and are pooled together in our analyses.

Microinjection

Glass capillaries (Harvard Apparatus glass capillaries with 780 μm inner diameter) are pulled using a needle puller and microforge to build a holding pipette and an injection needle. The resulting injection needles are filled with RNA and or protein solution diluted in injection buffer (5 mM Tris–HCl pH = 7.4, 0.1 mM EDTA) to the following concentrations: mCherry-EB3 100 ng/μl, Ect2-GFP, LifeAct-GFP, LifeAct-RFP, Lap2b-GFP and Cdc42T17N 200 ng/μl and Cdc42 reporter 150 ng/μl. To knock out Myo1c, zygotes were injected with 300 ng/μl Cas9 protein (IDT, 1081058) and 80 ng/μl gRNA1 and gRNA2 each diluted in injection buffer. The filled needle is positioned on a micromanipulator (Narishige MMO-4) and connected to a positive pressure pump (Eppendorf FemtoJet 4i). Embryos are placed in FHM drops covered with mineral oil under Leica TL Led microscope. Zygote or 2 cell-embryos were injected while holding with holding pipette connected to a Micropump CellTram Oil.

Micropipette aspiration

As described previously (Maître *et al*, 2015; Guevorkian & Maître, 2017), a microforged micropipette coupled to a microfluidic pump (Fluigent, MFCS EZ) is used to measure the surface tension of embryos. In brief, micropipettes of radii 8–16 μm are used to apply stepwise increasing pressures on the cell surface until reaching a deformation, which has the radius of the micropipette (R_p). At steady-state, the surface tension γ of the cell is calculated from the Young–Laplace's law applied between the cell and the micropipette: $\gamma = P_c/2\ (1/R_p - 1/R_c)$, where P_c is the critical pressure used to deform the cell of radius of curvature R_c.

Measurements of individual blastomeres from the same embryo are averaged and plotted as such.

Immunostaining

Embryos are fixed in 2% PFA (Euromedex, 2000-C) for 10 min at 37°C, washed in PBS and permeabilized in 0.01% Triton X-100 (Euromedex, T8787) in PBS (PBT) at room temperature before being placed in blocking solution (PBT with 3% BSA) at 4°C for 2–4 h. Primary antibodies (Table 1) are applied in blocking solution at 4°C overnight. After washes in PBT at room temperature, embryos are incubated with secondary antibodies, DAPI, and phalloidin (Table 1) in blocking solution at room temperature for 1 h. Embryos are washed in PBT and imaged in PBS–BSA immediately after.

Microscopy

Live imaging is performed using a Viventis Microscopy LS1 Live light-sheet microscope. Fluorescence excitation was achieved with a dual illumination scanned Gaussian beam light sheet of ~2.2 μm full width at half maximum using 488 and 561 nm lasers. Signal was collected with a Nikon CFI75 Apo LWD 25×/1.1 objective and through 525/50–25 or 561/25 band pass filter onto an Andor Zyla 4.2 Plus sCMOS camera. The microscope is equipped with an incubation chamber to keep the sample at 37°C and supply the atmosphere with 5% CO_2.

Surface tension measurements are performed on a Leica DMI6000 B inverted microscope equipped with a 40×/0.8 DRY HC PL APO Ph2 (11506383) objective and Retina R3 camera and 0.7× lens in front of the camera. The microscope is equipped with an incubation chamber to keep the sample at 37°C and supply the atmosphere with 5% CO_2.

Stained embryos are imaged on a Zeiss LSM900 Inverted Laser Scanning Confocal Microscope with Airyscan detector. Excitation is achieved using a 488 nm laser line through a 63×/1.4 OIL DICII PL APO objective. Emission is collected through a 525/50 band pass filter onto an airyscan photomultiplier (PMT) allowing to increase the resolution up to a factor 1.7.

Bioinformatic analysis

Mouse and human single cell RNA sequencing data were extracted from (Deng *et al*, 2014) and (Yan *et al*, 2013), analyzed as in (De Iaco *et al*, 2017). In brief, single cell RNAseq datasets of human and mouse embryos (GSE36552, GSE45719) were downloaded and analyzed using the online platform Galaxy (usegalaxy.org). The reads were aligned to the reference genome using TopHat (Galaxy Version 2.1.1 (Kim *et al*, 2013)) and read counts generated with htseq-count (Galaxy Version 0.9.1 (Anders *et al*, 2015)). Normalized counts were determined with limma-voom (Galaxy Version 3.38.3 + galaxy3 (Law *et al*, 2014)).

Data analysis

Image analysis

Fragment characterization

Using FIJI (Schindelin *et al*, 2012) to visualize individual confocal slices, fragments are identified as small spherical structures bounded by actin or membrane.

To measure fragment size, the confocal slice showing the largest fragment diameter is used and the contour of the membrane manually drawn.

The polar body, characterized by its presence from the zygote stage and intense DNA signal (much brighter than cells), was excluded from the analysis.

Cortical intensity measurements

FIJI is used to measure cortical intensity and distance to DNA. A segmented line is used to define the size and the location of the LifeAct or Myh9–GFP cap. Starting at the first division timepoint the intensity is measured at the segmented line, with the length of the eventually formed cap, and the distance between the center of the DNA mass and the center of the segmented line. The intensity of another segmented line drawn with the same length on a different part of the cell-medium interface where no cortical fluctuations are observed is used to normalize the intensity.

Spindle analysis

Spindle persistence was calculated by measuring the time between the appearance and disappearance of the spindle. Spindle straightness was measured using FIJI by dividing the length of a straight line connecting spindle poles divided by the length of a broken line drawn along the spindle. For spindle rotation, the angle between the initial direction of one spindle pole and its maximal change of direction was measured.

Nuclear envelope reassembly

The time between nuclear envelope disassembly and reassembly was measured based on the first time point where the nuclear envelope is not visible anymore until the time point where the nuclear envelope reappears. Cells from the same embryos are averaged together.

Statistics

Data are plotted using GraphPad Prism. Statistical tests are performed using GraphPad Prism. Statistical significance is considered when $P < 10^{-2}$.

The sample size was not predetermined and simply results from the repetition of experiments. No sample that survived the experiment, as assessed by the continuation of cell divisions, was excluded. No randomization method was used. The investigators were not blinded during experiments.

Data availability

The raw microscopy data and regions of interests (ROIs) are available on BioImage Archive (Sarkans *et al*, 2018): https://www.ebi.ac.uk/biostudies/bioimages/studies/S-BIAD725.

Expanded View for this article is available online.

Acknowledgements

We thank the imaging platform of the Genetics and Developmental Biology unit at the Institut Curie (PICT–IBiSA@BDD) for their outstanding support; the animal facility of the Institut Curie for their invaluable help. We thank Marie-Émilie Terret, Maria Almonacid, Marie-Hélène Verlhac, Kristine Schauer, Jean-Baptiste Brault, Martin Bähler, and Alexandre Baffet for sharing constructs and discussions. We thank Marie-Hélène Verlhac, Yohanns Bellaïche and members of the Maître lab for critical reading of the manuscript. Research in the lab of J-LM is supported by the Institut Curie, the Centre National de la Recherche Scientifique (CNRS), the Institut National de la Santé Et de la Recherche Médicale (INSERM), and is funded by grants from the ATIP–Avenir Program, the Fondation Schlumberger pour l'Éducation et la Recherche via the Fondation pour la Recherche Médicale, the European Research Council Starting Grant ERC-2017-StG 757557, the Agence Nationale de la Recherche (ANR-21-CE13-0010-02), the European Molecular Biology Organization Young Investigator program (EMBO YIP), the INSERM transversal program Human Development Cell Atlas (HuDeCA), Paris Sciences Lettres (PSL) QLife (17-CONV-0005) grant and Labex DEEP (ANR-11-LABX-0044) which are part of the IDEX PSL (ANR-10-IDEX-0001-02).

Author contributions

Diane Pelzer: Conceptualization; data curation; formal analysis; validation; investigation; visualization; methodology; writing – original draft; writing – review and editing. **Ludmilla de Plater:** Data curation; formal analysis; investigation; methodology. **Peta Bradbury:** Data curation; formal analysis; validation; visualization; writing – review and editing. **Adrien Eichmuller:** Methodology. **Anne Bourdais:** Methodology. **Guillaume Halet:** Supervision; methodology. **Jean-Léon Maître:** Conceptualization; data curation; formal analysis; supervision; funding acquisition; validation; investigation; visualization; methodology; writing – original draft; project administration; writing – review and editing.

Disclosure and competing interests statement

The authors declare that they have no conflict of interest.

References

Abdu Y, Maniscalco C, Heddleston JM, Chew T-L, Nance J (2016) Developmentally programmed germ cell remodelling by endodermal cell cannibalism. *Nat Cell Biol* 18: 1302 – 1310

Abe T, Kiyonari H, Shioi G, Inoue K, Nakao K, Aizawa S, Fujimori T (2011) Establishment of conditional reporter mouse lines at ROSA26 locus for live cell imaging. *Genesis* 49: 579 – 590

Alikani M (1999) Human embryo fragmentation in vitro and its implications for pregnancy and implantation. *Fertil Steril* 71: 836 – 842

Alikani M (2007) The origins and consequences of fragmentation in mammalian eggs and embryos. In *Human Preimplantation Embryo Selection*, Cohen J, Elder K (eds), pp 51 – 78. Boca Raton, FL: CRC Press

Anders S, Pyl PT, Huber W (2015) HTSeq—a python framework to work with high-throughput sequencing data. *Bioinformatics* 31: 166 – 169

Atkin-Smith GK, Poon IKH (2017) Disassembly of the dying: mechanisms and functions. *Trends Cell Biol* 27: 151 – 162

Bourdais A, Dehapiot B, Halet G (2022) MRCK controls myosin II activation in the polarized cortex of mouse oocytes and promotes spindle rotation and male pronucleus centration. *bioRxiv* https://doi.org/10.1101/2022.09.25.509421 [PREPRINT]

Capmany A, Yoshimura A, Kerdous R, Caorsi V, Lescure A, Nery ED, Coudrier E, Goud B, Schauer K (2019) MYO1C Stabilizes Actin and facilitates arrival of transport carriers at the Golgi apparatus. *J Cell Sci* 132: jcs.225029

Cavazza T, Takeda Y, Politi AZ, Aushev M, Aldag P, Baker C, Choudhary M, Bucevičius J, Lukinavičius G, Elder K *et al* (2021) Parental genome unification is highly error-prone in mammalian embryos. *Cell* 184: 2860 – 2877

Chavez SL, Loewke KE, Han J, Moussavi F, Colls P, Munne S, Behr B, Reijo Pera RA (2012) Dynamic blastomere behaviour reflects human embryo ploidy by the four-cell stage. *Nat Commun* 3: 1251

Cong L, Ran FA, Cox D, Lin S, Barretto R, Habib N, Hsu PD, Wu X, Jiang W, Marraffini LA *et al* (2013) Multiplex genome engineering using CRISPR/Cas systems. *Science* 339: 819 – 823

Currie CE, Ford E, Benham Whyte L, Taylor DM, Mihalas BP, Erent M, Marston AL, Hartshorne GM, McAinsh AD (2022) The first mitotic division of human embryos is highly error prone. *Nat Commun* 13: 6755

Daughtry BL, Rosenkrantz JL, Lazar NH, Fei SS, Redmayne N, Torkenczy KA, Adey A, Yan M, Gao L, Park B *et al* (2019) Single-cell sequencing of primate preimplantation embryos reveals chromosome elimination via cellular fragmentation and blastomere exclusion. *Genome Res* 29: 367 – 382

De Iaco A, Planet E, Coluccio A, Verp S, Duc J, Trono D (2017) DUX-family transcription factors regulate zygotic genome activation in placental mammals. *Nat Genet* 49: 941 – 945

Dehapiot B, Carrière V, Carroll J, Halet G (2013) Polarized Cdc42 activation promotes polar body protrusion and asymmetric division in mouse oocytes. *Dev Biol* 377: 202 – 212

Dehapiot B, Clément R, Bourdais A, Carrière V, Huet S, Halet G (2021) RhoA- and Cdc42-induced antagonistic forces underlie symmetry breaking and spindle rotation in mouse oocytes. *PLoS Biol* 19: e3001376

Deng M, Suraneni P, Schultz RM, Li R (2007) The Ran GTPase mediates chromatin signaling to control cortical polarity during polar body extrusion in mouse oocytes. *Dev Cell* 12: 301 – 308

Deng Q, Ramskold D, Reinius B, Sandberg R (2014) Single-cell RNA-seq reveals dynamic, random monoallelic gene expression in mammalian cells. *Science* 343: 193 – 196

Derrick R, Hickman C, Oliana O, Wilkinson T, Gwinnett D, Whyte LB, Carby A, Lavery S (2017) Perivitelline threads associated with fragments in human cleavage stage embryos observed through time-lapse microscopy. *Reprod Biomed Online* 35: 640 – 645

Dumont J, Petri S, Pellegrin F, Terret M-E, Bohnsack MT, Rassinier P, Georget V, Kalab P, Gruss OJ, Verlhac M-H (2007) A centriole- and RanGTP-independent spindle assembly pathway in meiosis I of vertebrate oocytes. *J Cell Biol* 176: 295 – 305

Firestone AJ, Weinger JS, Maldonado M, Barlan K, Langston LD, O'Donnell M, Gelfand VI, Kapoor TM, Chen JK (2012) Small-molecule inhibitors of the AAA+ ATPase motor cytoplasmic dynein. *Nature* 484: 125 – 129

Firmin J, Maître J-L (2021) Morphogenesis of the human preimplantation embryo: bringing mechanics to the clinics. *Semin Cell Dev Biol* 120: 22 – 31

Firmin J, Ecker N, Danon DR, Lange VB, Turlier H, Patrat C, Maitre J-L (2022) Mechanics of human embryo compaction. *bioRxiv* https://doi.org/10.1101/2022.01.09.475429 [PREPRINT]

Fujimoto VY, Browne RW, Bloom MS, Sakkas D, Alikani M (2011) Pathogenesis, developmental consequences, and clinical correlations of human embryo fragmentation. *Fertil Steril* 95: 1197 – 1204

Guevorkian K, Maître J-L (2017) Micropipette aspiration: a unique tool for exploring cell and tissue mechanics in vivo. *Methods Cell Biol* 139: 187 – 201

Halet G, Viard P, Carroll J (2008) Constitutive PtdIns(3,4,5)P3 synthesis promotes the development and survival of early mammalian embryos. *Development* 135: 425 – 429

Hardy K (1999) Apoptosis in the human embryo. *Rev Reprod* 4: 125 – 134

Hurst PR, Jefferies K, Eckstein P, Wheeler AG (1978) An ultrastructural study of preimplantation uterine embryos of the rhesus monkey. *J Anat* 126: 209 – 220

Jiang D, Jiang Z, Lu D, Wang X, Liang H, Zhang J, Meng Y, Li Y, Wu D, Huang Y *et al* (2019) Migrasomes provide regional cues for organ morphogenesis during zebrafish gastrulation. *Nat Cell Biol* 21: 1 – 17

Kalatova B, Jesenska R, Hlinka D, Dudas M (2015) Tripolar mitosis in human cells and embryos: occurrence, pathophysiology and medical implications. *Acta Histochem* 117: 111 – 125

Kim D, Pertea G, Trapnell C, Pimentel H, Kelley R, Salzberg SL (2013) TopHat2: accurate alignment of transcriptomes in the presence of insertions, deletions and gene fusions. *Genome Biol* 14: R36

Kiyomitsu T, Cheeseman IM (2013) Cortical dynein and asymmetric membrane elongation coordinately position the spindle in anaphase. *Cell* 154: 391 – 402

Kotak S, Busso C, Gönczy P (2012) Cortical dynein is critical for proper spindle positioning in human cells. *J Cell Biol* 199: 97 – 110

Labun K, Montague TG, Krause M, Torres Cleuren YN, Tjeldnes H, Valen E (2019) CHOPCHOP v3: expanding the CRISPR web toolbox beyond genome editing. *Nucleic Acids Res* 47: W171 – W174

Law CW, Chen Y, Shi W, Smyth GK (2014) Voom: precision weights unlock linear model analysis tools for RNA-seq read counts. *Genome Biol* 15: R29

Lebreton G, Géminard C, Lapraz F, Pyrpassopoulos S, Cerezo D, Spéder P, Ostap EM, Noselli S (2018) Molecular to organismal chirality is induced by the conserved myosin 1D. *Science* 362: 949 – 952

Lee Y, Hamann JC, Pellegrino M, Durgan J, Domart M-C, Collinson LM, Haynes CM, Florey O, Overholtzer M (2019) Entosis controls a developmental cell clearance in *C. elegans*. *Cell Rep* 26: 3212 – 3220

Maître J-L, Niwayama R, Turlier H, Nédélec F, Hiiragi T (2015) Pulsatile cell-autonomous contractility drives compaction in the mouse embryo. *Nat Cell Biol* 17: 849 – 855

Mangon A, Salaün D, Bouali ML, Kuzmić M, Quitard S, Thuault S, Isnardon D, Audebert S, Puech P-H, Verdier-Pinard P *et al* (2021) iASPP contributes to cell cortex rigidity, mitotic cell rounding, and spindle positioning. *J Cell Biol* 220: e202012002

Matthews HK, Delabre U, Rohn JL, Guck J, Kunda P, Baum B (2012) Changes in Ect2 localization couple actomyosin-dependent cell shape changes to mitotic progression. *Dev Cell* 23: 371 – 383

McIntosh BB, Ostap EM (2016) Myosin-I molecular motors at a glance. *J Cell Sci* 129: 2689 – 2695

Mori M, Yao T, Mishina T, Endoh H, Tanaka M, Yonezawa N, Shimamoto Y, Yonemura S, Yamagata K, Kitajima TS *et al* (2021) Rangtp and the Actin cytoskeleton keep paternal and maternal chromosomes apart during fertilization. *J Cell Biol* 220: e202012001

Muzumdar MD, Tasic B, Miyamichi K, Li L, Luo L (2007) A global double-fluorescent Cre reporter mouse. *Genesis* 45: 593 – 605

Özgüç Ö, de Plater L, Kapoor V, Tortorelli AF, Clark AG, Maître J-L (2022) Cortical softening elicits zygotic contractility during mouse preimplantation development. *PLoS Biol* 20: e3001593

Pereda J, Croxatto HB (1978) Ultrastructure of a seven-cell human embryo. *Biol Reprod* 18: 481 – 489

Plusa B, Piliszek A, Frankenberg S, Artus J, Hadjantonakis A-K (2008) Distinct sequential cell behaviours direct primitive endoderm formation in the mouse blastocyst. *Development* 135: 3081 – 3091

Ramkumar N, Patel JV, Anstatt J, Baum B (2021) Aurora B-dependent polarization of the cortical actomyosin network during mitotic exit. *EMBO Rep* 22: e52387

Riedl J, Crevenna AH, Kessenbrock K, Yu JH, Neukirchen D, Bista M, Bradke F, Jenne D, Holak TA, Werb Z *et al* (2008) Lifeact: a versatile marker to visualize F-Actin. *Nat Methods* 5: 605 – 607

Riedl J, Flynn KC, Raducanu A, Gärtner F, Beck G, Bösl M, Bradke F, Massberg S, Aszodi A, Sixt M *et al* (2010) Lifeact mice for studying F-Actin dynamics. *Nat Methods* 7: 168 – 169

Rodrigues NTL, Lekomtsev S, Jananji S, Kriston-Vizi J, Hickson GRX, Baum B (2015) Kinetochore-localized PP1–Sds22 couples chromosome segregation to polar relaxation. *Nature* 524: 489 – 492

Sarkans U, Gostev M, Athar A, Behrangi E, Melnichuk O, Ali A, Minguet J, Rada JC, Snow C, Tikhonov A *et al* (2018) The BioStudies database—one stop shop for all data supporting a life sciences study. *Nucleic Acids Res* 46: D1266 – D1270

Schindelin J, Arganda-Carreras I, Frise E, Kaynig V, Longair M, Pietzsch T, Preibisch S, Rueden C, Saalfeld S, Schmid B (2012) Fiji: an open-source platform for biological-image analysis. *Nat Methods* 9: 676 – 682

Sedzinski J, Biro M, Tinevez J-Y, Salbreux G, Paluch E (2011) Polar actomyosin contractility destabilizes the position of the cytokinetic furrow. *Nature* 476: 462 – 466

Simerly C, Nowak G, de Lanerolle P, Schatten G (1998) Differential expression and functions of cortical myosin IIA and IIB isotypes during meiotic maturation, fertilization, and mitosis in mouse oocytes and embryos. *Mol Biol Cell* 9: 2509 – 2525

Uraji J, Scheffler K, Schuh M (2018) Functions of Actin in mouse oocytes at a glance. *J Cell Sci* 131: jcs218099

Van Blerkom J, Davis P, Alexander S (2001) A microscopic and biochemical study of fragmentation phenotypes in stage-appropriate human embryos. *Hum Reprod* 16: 719 – 729

Wamaitha SE, Niakan KK (2018) Human pre-gastrulation development. *Curr Top Dev Biol* 128: 295 – 338

Wang H, Li Y, Yang J, Duan X, Kalab P, Sun SX, Li R (2020) Symmetry breaking in hydrodynamic forces drives meiotic spindle rotation in mammalian oocytes. *Sci Adv* 6: eaaz5004

Yan L, Yang M, Guo H, Yang L, Wu J, Li R, Liu P, Lian Y, Zheng X, Yan J *et al* (2013) Single-cell RNA-seq profiling of human preimplantation embryos and embryonic stem cells. *Nat Struct Mol Biol* 20: 1131 – 1139

Yumoto K, Shimura T, Mio Y (2020) Removing the zona pellucida can decrease cytoplasmic fragmentations in human embryos: a pilot study using 3PN embryos and time-lapse cinematography. *J Assist Reprod Genet* 37: 1349 – 1354

Zhang Y, Conti MA, Malide D, Dong F, Wang A, Shmist YA, Liu C, Zerfas P, Daniels MP, Chan C-C *et al* (2012) Mouse models of MYH9-related disease: mutations in nonmuscle myosin II-A. *Blood* 119: 238 – 250

